Title

Logarithm Diameter Scaling and Carrier Density Independence of One-Dimensional Luttinger Liquid Plasmon

Journal

Nano Letters, 19(4)

ISSN

1530-6984

Authors

Wang, Sheng
Wu, Fanqi
Zhao, Sihan
et al.

Publication Date

2019-04-10

DOI

10.1021/acs.nanolett.8b05031

Peer reviewed

Logarithm Diameter Scaling and Carrier Density Independence of One-dimensional Luttinger Liquid Plasmon

*Sheng Wang[1,2], Fanqi Wu[3], Sihan Zhao[1], Kenji Watanabe[4], Takashi Taniguchi[4], Chongwu Zhou[3,5], Feng Wang[1,2,6]**

[1]Department of Physics, University of California at Berkeley, Berkeley, California 94720, USA.

[2]Materials Science Division, Lawrence Berkeley National Laboratory, Berkeley, California 94720, USA.

[3]Department of Chemical Engineering and Materials Science, University of Southern California, Los Angeles, California 90089, USA

[4]National Institute for Materials Science, 1-1 Namiki, Tsukuba 305-0044, Japan.

[5]Department of Electrical Engineering, University of Southern California, Los Angeles, California 90089, USA

[6]Kavli Energy NanoSciences Institute at the University of California, Berkeley and the Lawrence Berkeley National Laboratory, Berkeley, California, 94720, USA.

*Correspondence to: fengwang76@berkeley.edu

Abstract: Quantum-confined electrons in one-dimensional (1D) metals are described by a Luttinger liquid. The collective charge excitations (i.e. plasmons) in a Luttinger liquid can behave qualitatively different from their conventional counterparts. For example, the Luttinger liquid plasmon velocity is uniquely determined by the electron-electron interaction, which scales logarithmly with the diameter of the 1D material. In addition, the Luttinger liquid plasmon is predicted to be independent on the carrier concentration. Here, we report the observation of such unusual Luttinger liquid plasmon behaviors in metallic single walled carbon nanotubes, a model system featuring strong electron quantum confinement. We systematically investigate the plasmon propagation in over 30 metallic carbon nanotubes of different diameters using infrared nanoscopy. We establish that the plasmon velocity has a weak logarithm dependence on the nanotube diameter, as predicted by the Luttinger liquid theory. We further study the plasmon excitation as a function of the carrier density in electrostatically gated metallic carbon nanotubes, and demonstrate that the plasmon velocity is completely independent on the carrier density. These behaviors are in striking contrast to conventional plasmons in 1D metallic shells, where the plasmon dispersion changes dramatically with the metal electron density and the 1D diameter. The unusual behaviors of Luttinger liquid plasmon may enable novel nanophotonic applications based on carbon nanotubes.

KEYWORDS: Luttinger liquid, Carbon nanotubes, Quantum plasmonics, Infrared nano-imaging

Introduction

Interacting electrons in three- and two-dimensional metals are well described by quasi-particles within the Fermi liquid theory. In one dimension (1D), however, Coulomb interactions qualitatively alter the electron behaviors and lead to a new type of correlated electron system — the Luttinger liquid[1-7]. Many novel phenomena can emerge in the Luttinger liquid, such as charge-spin separation, where the collective charge excitation (plasmon) and collective spin excitation (spinon) propagate independently at different velocities[8-10]. Metallic single walled carbon nanotubes (SWNTs) provide an ideal model system to study the Luttinger liquid behavior due to the strong electron quantum confinement in the lateral dimensions and the presence of different metallic nanotubes of varying chiralities and diameters[11-13]. It has been predicted that the electron-electron interaction strength, and therefore the Luttinger liquid plasmon excitation, has a logarithm dependence on the nanotube diameter. In addition, the electron density in SWNTs can be controlled conveniently through electrostatic gating in a field-effect transistor device configuration[14-17]. In spite of intense interests in the Luttinger liquid physics in SWNTs [18-23] [24, 25], the dependence of Luttinger liquid behavior on the nanotube diameter and the carrier density has never been explored experimentally.

In this Letter, we report the observation of logarithm diameter scaling and carrier density independence of Luttinger liquid plasmons in metallic SWNTs. We systematically investigate over 30 metallic SWNTs with different diameters using infrared nanoscopy. The plasmon velocities in SWNTs with diameters ranging from 0.7 nm to 1.8 nm are determined with a high

precision (within 3% uncertainty). Such high-precision measurements enabled us to reveal the weak but clearly observable logarithm diameter dependence of the plasmon velocity, which scales linearly with the Luttinger parameter g, as a function of the nanotube diameter. In addition, the study of plasmon excitation in gated metallic nanotubes shows that the plasmon velocity in metallic SWNTs has no dependence on carrier density. These plasmon signatures agree excellently with the Luttinger liquid theory and stand in stark contrast to plasmons in conventional metal nanostructures. The unusual behaviors are prime examples of quantum size effects in nanoscale plasmonic systems[26-28]. These in-depth understandings may enable novel nanophotonic applications based on carbon nanotubes.

Results and Discussion

Ultraclean SWNTs were directly grown on exfoliated hexagonal boron nitride (h-BN) flakes on silicon substrate with 285 nm oxide layers by chemical vapor deposition (CVD)[25, 29]. Different species of SWNTs on h-BN substrates can be grown by such CVD processes. Atomic force microscopy (AFM) characterization of the SWNTs shows that SWNTs with diameters ranging from 0.7 nm to 2.0 nm exist in our samples. Plasmons in these nanotubes were probed by means of an infrared scanning near-field optical microscopy (SNOM)[24, 25, 30-32]. This infrared nano-imaging technique is based on a tapping mode AFM. Infrared light with wavelength 10.6 μm is focused onto the apex of a gold coated AFM tip. The sharp tip with its large momentum enables the excitation of plasmons and simultaneously scatters this plasmon field to the far field, which is captured by an HgCdTe detector. The excited plasmon wave propagates along the nanotubes and get reflected by nanotube ends or other scatters. The interference between the tip-launched plasmon field and the reflected plasmon field produces a periodic electric field distribution. Probing of this periodic electric field by scanning the tip along the nanotube enables the direct visualization of the propagating plasmon waves.

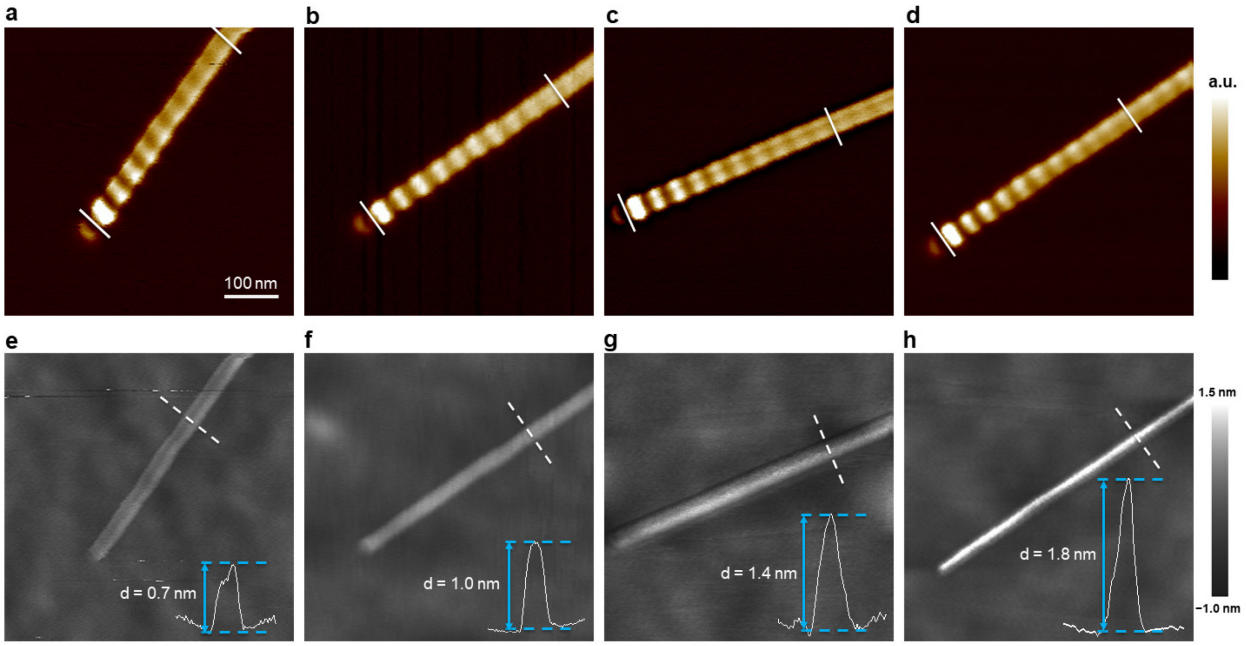

Figure 1. Correlation of near-field optical response and nanotube size in various metallic SWNTs. (a) to **(d)** Near-field images of representative metallic SWNTs with varying diameters. Prominent oscillation peaks persist in various metallic SWNTs. **(e)** to **(h)** Corresponding topography images to the near-field images above. Insets are the line profiles across SWNTs along the white dashed lines. From the height profiles, diameters of nanotubes in (e) to (g) are determined to be 0.7 nm, 1.0 nm, 1.4 nm, 1.8 nm, respectively. Note that all images share the same scale bar as shown in (a) for direct comparison.

Figures 1a-d display infrared nano-imaging results of representative metallic SWNTs with varying diameters. It's evident that prominent oscillations persist in these different metallic SWNTs. The oscillation peaks in the near-field images correspond to the constructive interference between the plasmon wave excited by the tip and that reflected by the end of the nanotube. The plasmon wavelength λ_p thus can be simply determined as twice the separation between adjacent peaks in the near-field images. Plasmon velocity can then be readily acquired as $v_p = \lambda_p f$ where f ~ 28.3 THz is the frequency of the excitation light. The diameters of the SWNTs can be determined from the topography images, which are obtained simultaneously with near-field images during the scanning. Figures 1e-h show the topography images corresponding to the near-field images Figures 1a-d. Insets are the line profiles across SWNTs taken along the white dashed lines. From the height profiles, diameters of SWNTs in Figures 1e-h are determined to be 0.7 nm, 1.0 nm, 1.4 nm, 1.8 nm, respectively. Correlation of the near-field optical response and the structural property enables a systematic revelation of the size dependence of the plasmon velocity.

To better present the measured data, we plot in Figure 2a (solid lines) the near-field response

profiles taken along the nanotubes between two white bars in the near-field images Figures 1a-d. Plasmon wavelength equal to twice the oscillation period is marked by the black double arrow. From the near-field response profiles, it's clearly seen that the plasmon wavelength decreases as diameter increases. This trend is in sharp contrast to conventional 1D metal nanoshells with electrons described by the Drude model. Plasmon wavelength in a 1D metal nanoshell under the Drude model has been theoretically predicted to increase almost in a linear fashion as diameter increases[33, 34]. Experimentally, plasmon wavelength in 1D metallic nanowires has been observed to increase dramatically with increasing diameter[35]. The different trend highlights the unique quantum nature of 1D plasmons in metallic SWNTs.

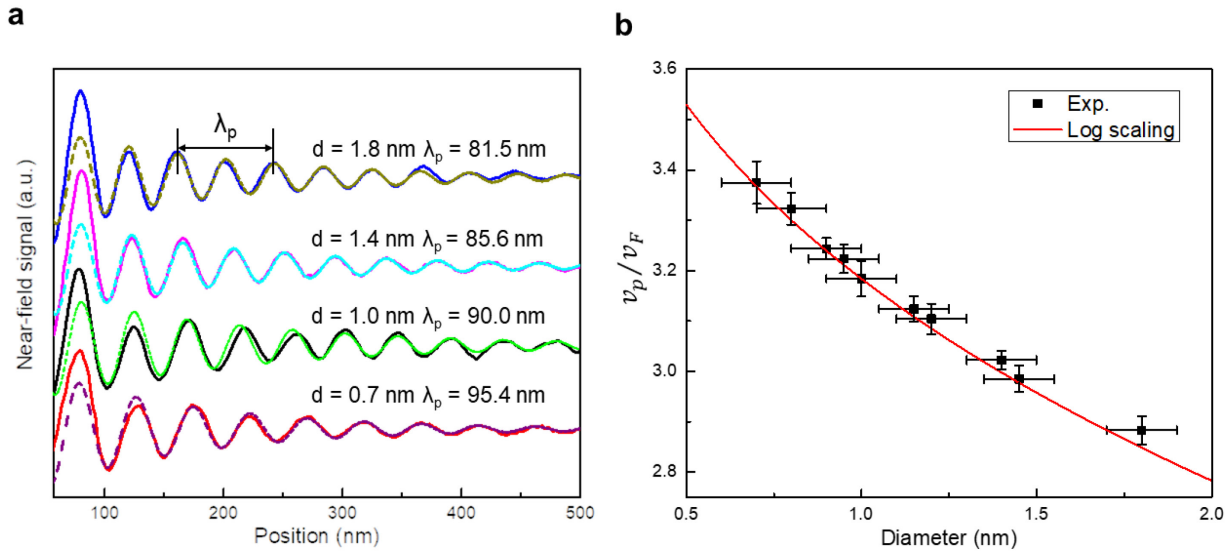

Figure 2. Logarithmic diameter dependence of the plasmon velocity. (a) Near-field response line profiles and extraction of plasmon wavelength. Solid lines represent the near-field profiles taken along SWNTs between two white bars in the near-field images Figures 1a-d. Plasmon wavelength equal to twice the oscillation period in the near-field images is marked by the black double arrow. We can extract both the plasmon wavelength λ_P and quality factor Q as a function of diameter by fitting the line profiles with a damped oscillator form $e^{-2\pi x/(Q\cdot\lambda_P)}\sin\left((4\pi x)/\lambda_p\right)$ from the nanotube end. The fitting curves for each diameter are shown in dashed lines. **(b)** The experimental data (black squares) agree excellently with a logarithmic diameter dependence (red curve). Horizontal errors bars reflect the precision with which diameter can be determined from the AFM topography measurements. Vertical error bars indicate a 95% confidence interval determined from the curve fitting of the near-field profiles with a damped oscillator form.

Near-field line profiles along the nanotubes represented by the solid lines in Figure 2a reveal how the plasmon wave gets damped as it propagates. For a quantitative study, we can extract both the plasmon wavelength λ_P and quality factor Q as a function of diameter by fitting the line profiles with a damped oscillator form $e^{-2\pi x/(Q\cdot\lambda_P)}\sin\left((4\pi x)/\lambda_p\right)$ from the nanotube end[24,

[25]. The fitting curves for each diameter are shown in dashed lines in Figure 2a. In our measured diameter range from 0.7 nm to 1.8 nm, plasmon wavelength λ_p is determined to be from 95.4 nm to 81.5 nm with a 95% confidence interval of ~ 2.0 nm from the fitting. Plasmon velocity are then easily calculated as $v_p = \lambda_p f \sim 2.7 \times 10^6\, m/s$ to $2.3 \times 10^6\, m/s$ where f ~ 28.3 THz is the frequency of the excitation light. In metallic SWNTs, $v_F \sim 0.8 \times 10^6\, m/s$ is the Fermi velocity. Figure 2b summarizes the dependence of plasmon velocity in terms of v_p/v_F on diameter for metallic SWNTs with an ample range of diameters including those shown in Figure 1. Horizontal error bars reflect the precision with which diameter can be determined from the AFM topography measurement. Vertical error bars indicate the uncertainty from the fitting. These data points can be explicitly compared with predictions by the Luttinger liquid theory. For an individual SWNT of diameter d residing on a substrate, the Luttinger liquid theory predicts the Luttinger liquid interaction parameter g to be[12, 24]

$$\frac{1}{g} = \frac{v_p}{v_F} = \sqrt{1 + \frac{8e^2}{4\pi\varepsilon_{eff}\pi\hbar v_F} \mathrm{In}(\frac{\lambda_p}{\pi d})} \quad (1)$$

where v_p is the velocity of the collective charge mode, i.e. plasmon velocity, $v_F \sim 0.8 \times 10^6\, m/s$ is the Fermi velocity, ε_{eff} is the effective dielectric constant due to substrate screening and the plasmon wavelength λ_p determines the cutoff length of the Coulomb interactions and acts as the screening length. The second term arises from the long-range Coulomb interaction which goes as $q^2/2C$, where $C \sim 2\pi\varepsilon_{eff}/In(\frac{\lambda_p}{\pi d})$ is the capacitance per unit length. Therefore, the electron-electron interaction in the Luttinger liquid exhibits a logarithm scaling with the nanotube diameter. In our measured diameter range from 0.7 nm to 1.8 nm, plasmon velocity v_p has been obtained to be from $2.7 \times 10^6\, m/s$ to $2.3 \times 10^6\, m/s$. The Luttinger liquid parameter g describing the interaction in SWNTs can then also be determined to be $g = v_F/v_p \sim 0.29$ to 0.34, which indicates strong Coulomb repulsion between electrons in all studied metallic SWNTs. Because interaction energy dominates in studied metallic SWNTs, we can safely neglect the first term in equation (1). The plasmon velocity thus becomes $v_p = \sqrt{\frac{8e^2 v_F}{4\pi\varepsilon_{eff}\pi\hbar} \mathrm{In}(\frac{\lambda_p}{\pi d})} \propto \sqrt{\mathrm{In}(\frac{\lambda_p}{\pi d})}$. Note that plasmon wavelength λ_p also varies with diameter but the change (~ 16%) is much smaller compared to the change in diameter (more than 100%). This predicted logarithmic dependence on the diameter is depicted in Figure 2b by the red curve, which shows excellent agreement with the experimental results represented by the black squares.

We next systematically investigate the dependence of plasmon behaviors on carrier density in metallic SWNTs. Figure 3a illustrates the schematic of infrared nano-imaging of SWNTs with carrier density controlled by applying a back gate voltage V_g. In order to observe the prominent Luttinger liquid plasmon oscillations by our infrared nano-imaging technique, we utilize the nanotube end as a well-defined reflector to create the standing plasmon wave. Therefore, we are not able to use a two-terminal nanotube device for the near-field measurements. However, the

metallic nanotubes are sitting on hBN substrates and their charge neutral points tend to be close to a zero gate voltage. To make sure that this is the case, we have carried out electrical transport measurements for many two-terminal metallic nanotube devices fabricated using exactly the same procedures. Representative electrical transport data for two-terminal metallic nanotube devices are shown in Figure S2. These transport data clearly show that the metallic nanotubes can be gated efficiently by the back gate and the charge neutral points tend to be relatively close to zero gate voltage and within our measured voltage range. When gate voltage V_g is varied from −20 V to 30 V, the carrier type in carbon nanotubes changes from hole doping to charge neutrality and then to electron doping. The near-field optical responses at these different gate voltages are shown in Figures 3c-h. It's evident that prominent plasmons are excited at different gate voltages or carrier densities. Line profiles along the nanotube in the near-field images Figures 3c-h for different gate voltages are plotted in Figure S1. Plasmon wavelength determined as twice the oscillation period and plasmon amplitude reflected in the near-field intensity are largely independent on gate voltages.

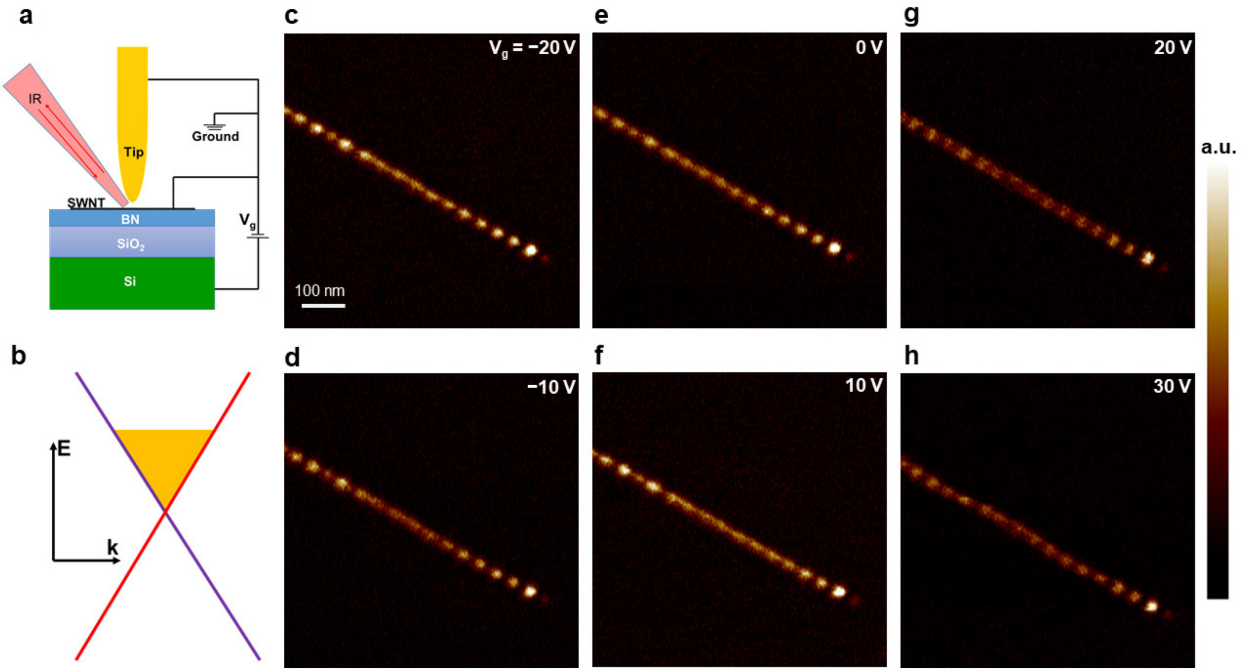

Figure 3. Infrared nano-imaging of an electrostatically gated metallic nanotube. (a) Schematic of infrared nano-imaging of a nanotube with carrier density controlled by applying a back gate voltage V_g. **(b)** Illustrative band diagram of metallic SWNTs. With this linear dispersion and 1D nature, the Fermi velocity as well as the density of state remains a constant independent on the Fermi energy. **(c)** to **(h)** Near-field responses of a metallic SWNT at different gate voltages. From **(c)** to **(h)**, the gate voltage is varied from −20 V to 30 V and the nanotube changes from hole doping to charge neutrality and then to electron doping. Plasmon wavelength determined as twice the oscillation period and plasmon amplitude reflected in the near-field intensity are largely independent on gate voltages.

Note that even at around charge neutrality (Figures 3d-e), the plasmon oscillations still exist and behave the same way as the highly doped ones (Figure 3h). This counter-intuitive carrier density independent plasmon behavior in metallic nanotubes stands in striking contrast to conventional plasmons. In conventional 2D or 3D systems, plasmon wavelength and amplitude are closely associated with the carrier density for a given frequency. For instance, plasmons in graphene have been demonstrated to be continuously tuned by changing gate voltages[30-32]. This peculiar plasmon behavior in metallic SWNTs arises from its unique 1D massless Dirac electrons. Figure 3b illustrates the band diagram of a metallic SWNT which features a linear dispersion. With this linear dispersion and 1D nature, the Fermi velocity as well as the density of state remains a constant independent on the Fermi energy. Quantum excitations including the plasmons of an electron liquid close to the Fermi energy are determined by the Fermi velocity and density of state rather than the total carrier concentration. The plasmon excitation in metallic SWNTs therefore shows no dependence on carrier density. The peculiar behavior is also explicitly evident in the prediction by the Luttinger liquid theory as shown in equation (1). It's clear from the prediction that plasmon wavelength is a function of only the Fermi velocity for a given nanotube under certain dielectric environment. Because Fermi velocity is a constant in metallic SWNTs with linear dispersion, the plasmon behaviors will remain exactly the same regardless of carrier density.

Conclusion

In summary, we report the observation of peculiar Luttinger liquid plasmon signatures in metallic SWNTs, including an intriguing logarithmic dependence of plasmon wavelength on diameter and a counter-intuitive independence on carrier density. These signatures stand in stark contrast to conventional plasmons and are prime examples of quantum size effects in nanoscale plasmonic systems. Our findings not only provide fundamental insight into Luttinger liquid physics in 1D systems but also pave the way for promising nanophotonic applications based on SWNTs.

ASSOCIATED CONTENT

Supporting Information.

(1) Line profiles of gate dependent infrared nano-imaging measurements in Figure 3, (2) Representative electrical transport data for two-terminal metallic nanotube devices, (3) Quality factor as a function of diameter for metallic nanotubes in Figure 2, (4) Discussion of Random phase approximation theory. This material is available free of charge via the Internet at http://pubs.acs.org.

Corresponding Author: fengwang76@berkeley.edu (F.W.)

Author contributions: F.W. and S.W. conceived the project and designed the experiment. F.W. and C.Z supervised the project. S.W. fabricated the devices and performed infrared nano-imaging measurements. S.W. and F.W. analyzed the data. Fanqi W. under the supervision of C.Z. grew the SWNTs samples. S.Z. and S.W. fabricated the devices for transport measurements and performed the electrical transport measurements. K.W. and T.T. provided the h-BN crystals. All authors contributed to the discussion of the results and the writing of the manuscript.

Funding Sources: This work was mainly supported by the Director, Office of Science, Office of Basic Energy Sciences, Materials Sciences and Engineering Division of the U.S. Department of Energy under Contract No. DE-AC02-05-CH11231 (sp2-Bonded Materials Program KC2207). The device fabrication was supported by the Office of Naval research (MURI award N00014-16-1-2921). The data analysis was supported by the NSF award 1808635. Fanqi W. and C.Z. acknowledge National Science Foundation for financial support under Grant No. 769K521. K.W. and T.T. acknowledge support from the Elemental Strategy Initiative conducted by the MEXT, Japan and the CREST (JPMJCR15F3), JST.

References:

1. Tomonaga, S.-i. *Remarks on Bloch's method of sound waves applied to many-fermion problems*. *Progress of Theoretical Physics* **1950,** 5, (4), 544-569.

2. Luttinger, J. M. *An Exactly Soluble Model of a Many-Fermion System*. *Journal of Mathematical Physics* **1963,** 4, (9), 1154.

3. Haldane, F. D. M. *'Luttinger liquid theory' of one-dimensional quantum fluids. I. Properties of the Luttinger model and their extension to the general 1D interacting spinless Fermi gas*. *Journal of Physics C: Solid State Physics* **1981,** 14, (19), 2585.

4. Giamarchi, T., *Quantum physics in one dimension*. Oxford university press: Oxford, 2004; Vol. 121.

5. Deshpande, V. V.; Bockrath, M.; Glazman, L. I.; Yacoby, A. *Electron liquids and solids in one dimension*. *Nature* **2010,** 464, (7286), 209-216.

6. Voit, J. *One-Dimensional Fermi Liquids*. *Reports on Progress in Physics* **1995,** 58, (9), 977-1116.

7. Giuliani, G.; Vignale, G. *Quantum Theory of the Electron Liquid*. Cambridge University Press: Cambridge, 2005; pp 501-549.

8. Lee, J.; Eggert, S.; Kim, H.; Kahng, S. J.; Shinohara, H.; Kuk, Y. *Real Space Imaging of One-Dimensional Standing Waves: Direct Evidence for a Luttinger Liquid*. *Physical Review Letters* **2004,** 93, (16), 166403.

9. Jompol, Y.; Ford, C. J. B.; Griffiths, J. P.; Farrer, I.; Jones, G. A. C.; Anderson, D.; Ritchie, D. A.; Silk, T. W.; Schofield, A. J. *Probing Spin-Charge Separation in a Tomonaga-Luttinger Liquid*. *Science* **2009,** 325, (5940), 597-601.

10. Hashisaka, M.; Hiyama, N.; Akiho, T.; Muraki, K.; Fujisawa, T. *Waveform measurement of charge- and spin-density wavepackets in a chiral Tomonaga–Luttinger liquid*. *Nature Physics* **2017,** 13, 559.

11. Saito, R.; Dresselhaus, G.; Dresselhaus, M. S. *Physical Properties of Carbon Nanotube*. Imperial College Press: London, 1998.

12. Kane, C.; Balents, L.; Fisher, M. P. A. *Coulomb interactions and mesoscopic effects in carbon nanotubes*.

Physical Review Letters **1997,** 79, (25), 5086-5089.

13. Egger, R.; Gogolin, A. O. *Effective Low-Energy Theory for Correlated Carbon Nanotubes*. *Physical Review Letters* **1997,** 79, (25), 5082-5085.

14. Tans, S. J.; Devoret, M. H.; Dai, H.; Thess, A.; Smalley, R. E.; Geerligs, L. J.; Dekker, C. *Individual single-wall carbon nanotubes as quantum wires*. *Nature* **1997,** 386, (6624), 474-477.

15. Tans, S. J.; Verschueren, A. R. M.; Dekker, C. *Room-temperature transistor based on a single carbon nanotube*. *Nature* **1998,** 393, 49.

16. Purewal, M. S.; Hong, B. H.; Ravi, A.; Chandra, B.; Hone, J.; Kim, P. *Scaling of Resistance and Electron Mean Free Path of Single-Walled Carbon Nanotubes*. *Physical Review Letters* **2007,** 98, (18), 186808.

17. Javey, A.; Guo, J.; Wang, Q.; Lundstrom, M.; Dai, H. *Ballistic carbon nanotube field-effect transistors*. *Nature* **2003,** 424, (6949), 654-657.

18. Bockrath, M.; Cobden, D. H.; McEuen, P. L.; Chopra, N. G.; Zettl, A.; Thess, A.; Smalley, R. E. *Single-electron transport in ropes of carbon nanotubes*. *Science* **1997,** 275, (5308), 1922-1925.

19. Bockrath, M.; Cobden, D. H.; Lu, J.; Rinzler, A. G.; Smalley, R. E.; Balents, L.; McEuen, P. L. *Luttinger-liquid behaviour in carbon nanotubes*. *Nature* **1999,** 397, (6720), 598-601.

20. Yao, Z.; Postma, H. W. C.; Balents, L.; Dekker, C. *Carbon nanotube intramolecular junctions*. *Nature* **1999,** 402, (6759), 273-276.

21. Ishii, H.; Kataura, H.; Shiozawa, H.; Yoshioka, H.; Otsubo, H.; Takayama, Y.; Miyahara, T.; Suzuki, S.; Achiba, Y.; Nakatake, M.; Narimura, T.; Higashiguchi, M.; Shimada, K.; Namatame, H.; Taniguchi, M. *Direct observation of Tomonaga-Luttinger-liquid state in carbon nanotubes at low temperatures*. *Nature* **2003,** 426, (6966), 540-544.

22. Gao, B.; Komnik, A.; Egger, R.; Glattli, D. C.; Bachtold, A. *Evidence for Luttinger-Liquid Behavior in Crossed Metallic Single-Wall Nanotubes*. *Physical Review Letters* **2004,** 92, (21), 216804.

23. Kim, N. Y.; Recher, P.; Oliver, W. D.; Yamamoto, Y.; Kong, J.; Dai, H. *Tomonaga-Luttinger Liquid Features in Ballistic Single-Walled Carbon Nanotubes: Conductance and Shot Noise*. *Physical Review Letters* **2007,** 99, (3), 036802.

24. Shi, Z.; Hong, X.; Bechtel, H. A.; Zeng, B.; Martin, M. C.; Watanabe, K.; Taniguchi, T.; Shen, Y.-R.; Wang, F. *Observation of a Luttinger-liquid plasmon in metallic single-walled carbon nanotubes*. *Nature Photonics* **2015,** 9, (8), 515-519.

25. Zhao, S.; Wang, S.; Wu, F.; Shi, W.; Utama, I. B.; Lyu, T.; Jiang, L.; Su, Y.; Wang, S.; Watanabe, K.; Taniguchi, T.; Zettl, A.; Zhang, X.; Zhou, C.; Wang, F. *Correlation of Electron Tunneling and Plasmon Propagation in a Luttinger Liquid*. *Physical Review Letters* **2018,** 121, (4), 047702.

26. Scholl, J. A.; Koh, A. L.; Dionne, J. A. *Quantum plasmon resonances of individual metallic nanoparticles*. *Nature* **2012,** 483, 421.

27. Halperin, W. P. *Quantum size effects in metal particles*. *Reviews of Modern Physics* **1986,** 58, (3), 533-606.

28. Campos, A.; Troc, N.; Cottancin, E.; Pellarin, M.; Weissker, H.-C.; Lermé, J.; Kociak, M.; Hillenkamp, M. *Plasmonic quantum size effects in silver nanoparticles are dominated by interfaces and local environments*. *Nature Physics* **2019,** 15, (3), 275-280.

29. Liu, B.; Wu, F.; Gui, H.; Zheng, M.; Zhou, C. *Chirality-Controlled Synthesis and Applications of Single-Wall Carbon Nanotubes*. *ACS Nano* **2017,** 11, (1), 31-53.

30. Chen, J.; Badioli, M.; Alonso-Gonzalez, P.; Thongrattanasiri, S.; Huth, F.; Osmond, J.; Spasenovic, M.; Centeno, A.; Pesquera, A.; Godignon, P.; Zurutuza Elorza, A.; Camara, N.; de Abajo, F. J. G.; Hillenbrand, R.; Koppens, F. H. L.

Optical nano-imaging of gate-tunable graphene plasmons. *Nature* **2012,** 487, (7405), 77-81.

31. Fei, Z.; Rodin, A. S.; Andreev, G. O.; Bao, W.; McLeod, A. S.; Wagner, M.; Zhang, L. M.; Zhao, Z.; Thiemens, M.; Dominguez, G.; Fogler, M. M.; Neto, A. H. C.; Lau, C. N.; Keilmann, F.; Basov, D. N. *Gate-tuning of graphene plasmons revealed by infrared nano-imaging*. *Nature* **2012,** 487, (7405), 82-85.

32. Kang, J.-H.; Wang, S.; Shi, Z.; Zhao, W.; Yablonovitch, E.; Wang, F. *Goos-Hänchen Shift and Even–Odd Peak Oscillations in Edge-Reflections of Surface Polaritons in Atomically Thin Crystals*. *Nano Letters* **2017,** 17, (3), 1768-1774.

33. Takahara, J.; Yamagishi, S.; Taki, H.; Morimoto, A.; Kobayashi, T. *Guiding of a one-dimensional optical beam with nanometer diameter*. *Opt. Lett.* **1997,** 22, (7), 475-477.

34. Soleymani, S.; Golmohammadi, S. *Surface Plasmon Polaritons Propagation Along Armchair and Zigzag Single-Wall Carbon Nanotubes With Different Radii*. *IEEE Transactions on Nanotechnology* **2017,** 16, (2), 307-314.

35. Wei, H.; Zhang, S.; Tian, X.; Xu, H. *Highly tunable propagating surface plasmons on supported silver nanowires*. *Proceedings of the National Academy of Sciences* **2013,** 110, (12), 4494-4499.

Graphic for the table of contents: